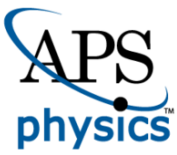

This is the accepted manuscript made available via CHORUS. The article has been published as:

Broadband passive nonlinear acoustic diode

Amir Darabi, Lezheng Fang, Alireza Mojahed, Matthew D. Fronk, Alexander F. Vakakis, and Michael J. Leamy

Phys. Rev. B **99**, 214305 — Published 20 June 2019

DOI: 10.1103/PhysRevB.99.214305

Broadband passive nonlinear acoustic diode

Amir Darabi,* Lezheng Fang,* Alireza Mojahed,† Matthew D. Fronk,* Alexander F. Vakakis,‡ and Michael J. Leamy§

In dynamical and acoustical systems, breaking reciprocity is achievable by employing external biases, spatial temporal variations of material properties, or nonlinearities. In this present work, we propose, theoretically analyze, and experimentally demonstrate the first passive broad-band mechanical diode, by adding an asymmetric local nonlinear interface to an otherwise linear wave-guide. It is shown that for a broad range of input energies and frequencies, three different types of non-reciprocal behaviors are obtained, i) different transmitted energies depending on the direction of wave propagation, ii) transmission of acoustic waves allowed in one direction but not in the reverse direction, and iii) arrest of propagating waves at the nonlinear interface only in one (preferred) direction. A unique feature of the proposed acoustic device compared to previous designs, is its capability to achieve passive non-reciprocity without altering or distorting the frequency content of the sending signal. The proposed system can pave the way for designing passive acoustic or thermal diodes, and adaptable non-reciprocal wave transmission devices of enhanced robustness that are tunable with, and passively adaptive to energy.

Originated from Onsager-Casimir principle of microscopic reversibility [1, 2], in a linear time-invariant (LTI) system, acoustic reciprocity is defined as a symmetrical wave transmission from a source to a receiver by exchanging their positions [3, 4]. In contrast, non-reciprocity violates this property to enable the control of wave propagation in a desired direction [5]. Motivated by the electric diode, recently, acoustic non-reciprocity has received significant attention due to applications in biomedical ultrasound devices [5, 6], energy harvesting metamaterials [7, 8], thermal computers [9–11], and direction dependent topological insulators [12–14].

Achieving non-reciprocity in mechanical systems is obtained by two different techniques: i) breaking time reversal symmetry in linear systems (active) [15–19], and ii) incorporating nonlinearity to create configurational asymmetry (passive) [20–22]. Breaking time-reversal symmetry for linear systems has been studied theoretically and experimentally in the past few years by employing external controllers [23–25]. Non-reciprocity in these devices was obtained by using uni-rotational circulating fluids [12], spatial temporal variation of the material properties [26, 27], or piezo-structures in electroacoustic devices [28, 29]. As discussed earlier, all of these reviewed works need an active element to control the response of the system continuously.

On the other hand, achieving non-reciprocity by passive means for mechanical devices has been given less consideration. One possible technique to break reciprocity passively is to utilize both nonlinearity and asymmetry in a periodic metamaterial [30]. These systems introduce energy dependent dispersion and group velocity relationship to design acoustic filters, switches, and diodes [20, 31]. Boechler *et al.* experimentally presented the first bifurcation-based acoustic rectifier and switch in a granular chain with a point defect to generate waves at lower frequencies which fall within the band-pass of the structure [25]. However, location of the interface relative to the source limits the application of the design for sound and vibration isolation. To overcome this issue, Grinberg *et al.* proposed a device by employing vibro-impact elements to break reciprocity, where two unequal grounding springs provided the necessary asymmetry in the system [32]. Most recently, Moore and Fronk *et al.* theoretically analyzed and experimentally demonstrated passive acoustic diodes based on irreversible nonlinear energy transfers from large to small scales in a periodic system [33–35]. Most of these reviewed devices are either narrow-band or alter and distort the frequency content of the sending signal significantly, which raises difficulties in applicability of the design.

In this work, we propose and experimentally verify a simple, passive, and highly effective nonlinear acoustic diode for broad frequency and energy ranges with minimal distortion of the acoustic signal. The proposed system is composed of two linear wave-guides connected by a nonlinear interface, where three unequal masses are attached by strongly nonlinear springs to provide local asymmetry. We demonstrate that the considered asymmetry in the nonlinear region is crucial to achieving a non-reciprocal response. The presented structure provides three different types of non-reciprocal behavior based on energy and frequency range of operation: i) the amount of transmitted energy in opposite directions is significantly different without distorting the frequency of the input signal, ii) waves are partially transmitted in one direction with minimal frequency distortion, but propagation in the other direction is prevented, and iii) transmitted waves are arrested at the location of the nonlinear interface only for one propagation direction. This latter non-reciprocity (yielding energy localization)

* Woodruff School of Mechanical Engineering, Georgia Institute of Technology, Atlanta, GA
† Department of Mechanical Science and Engineering, University of Illinois at Urbana- Champaign, Champaign, IL
‡ Department of Mechanical Science and Engineering, University of Illinois at Urbana- Champaign, Champaign, IL ; avakakis@illinois.edu
§ Woodruff School of Mechanical Engineering, Georgia Institute of Technology, Atlanta, GA; michael.leamy@me.gatech.edu

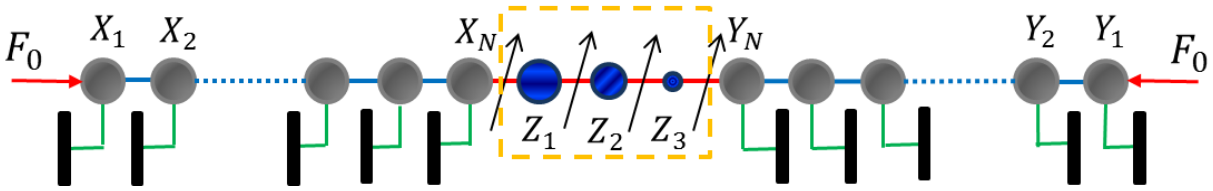

FIG. 1. **System model.** Schematic of a 1D chain composed of two identical linear wave-guides and a connecting nonlinear interface (blue masses marked with orange dashed lines). Each linear domain (i.e., wave-guide) contains N grounded masses (green connections) connected through linear springs (blue connections). For the nonlinear domain, three different masses are connected through nonlinear springs (red connections with black arrows). A harmonic force F_0 at each end provides equal and opposite forces to initiate waves into the system. Note that, none of the masses at the nonlinear interface are grounded.

can be used to dissipate the unwanted vibrational energy through resonance capture with minimal back-scattering for applications in vibration and shock isolation [36, 37], dynamic instability suppression [38], vortex induced vibration control [39, 40], control of Bouc-Wen structures [41], and acoustic mitigation [42, 43].

I. RESULTS

A. Numerical results

Figure 1 displays the system capturing the essential ideas of the system. As depicted, two identical linear wave-guides each containing $N = 100$ masses are connected through a nonlinear interface composed of three different masses which are coupled to each other by cubic springs. For the linear domains, all the masses M, are connected using linear springs k, and grounding springs k_g, respectively. Considering the system from left to right, M_1, M_2, M_3 denote masses, and k_{NL1}, k_{NL2}, k_{NL3}, k_{NL4} denote the cubic springs in the nonlinear domain. These mass variation from left to right provides asymmetry in the nonlinear domain, which is necessary to achieve non-reciprocity [30]. To reduce the complexity in the system, new parameters have been defined as below,

$$M = M_1 = m; M_3 = \epsilon M_2 = \epsilon^2 m, \tag{1}$$

$$k_{NL4} = \beta k_{NL3} = \beta^2 k_{NL2} = \beta^3 k_{NL1}, \tag{2}$$

where ϵ, and β are two new parameters to define the asymmetry, and nonlinearity in the structure. Furthermore, for simplicity, all other parameters in the system are normalized as follow,

$$\omega_0 = \sqrt{\frac{k_g}{m}}; t = \tau\omega_0; k_1 = \frac{k}{m\omega_0^2}; \alpha = \frac{k_{NL}}{m\omega_0^2}. \tag{3}$$

Full details on deriving equations of motion and dispersion relationships of the linear wave-guides are provided in Supplementary Note 1 [**?**].

For the system presented in this study, waves are initiated at either end of the whole wave-guide. The initiated waves then travel along the linear domain until they reach the nonlinear interface. After reaching the first mass in the nonlinear domain, a portion of the wave energy will be transmitted through the connection, and the rest will be reflected back. The normalized amount of energy for each domain is defined as below,

$$\eta_i = \frac{E_i}{E_{tot}}, \tag{4}$$

where E_i represents the energy of the considered domain, and E_{tot} denotes the total energy in the system, respectively. When the system is excited on the left end, the initial waves travel from left to right (LR), and the normalized transmitted energy is the energy of the right wave-guide (η_R), while when the harmonic force is applied on the right end of the system, waves travel from right to left (RL) and the transmitted energy is the energy of the left wave-guide (η_L). For all the numerical results presented in this section, the system parameter values are $\omega_0 = m = k_1 = \alpha = 1$, and $\epsilon = \sqrt{0.1}$. Supplementary Note 2 provides details on numerical modeling, energy calculations, and discussion on choosing system parameters.

Figure 2 demonstrates the normalized transmitted energy by sweeping input amplitude and frequency for two different systems. For the top figures, the nonlinear springs in Fig. 1 are replaced by purely linear springs (k_1), while the bottom figures plot the normalized transmitted energy for the system with nonlinear connections. As observed, for a purely linear system with an asymmetrical configuration, reciprocal behavior is documented; this documents the necessity of nonlinearity to achieve a non-reciprocal response. As depicted in bottom figures, for broad ranges of input force and frequency, the system behaves differently for opposite wave directions.

For small enough input force amplitudes ($F_0 < 0.5N$), the restoring forces in the nonlinear springs are significantly smaller than the linear springs ($F_{NL}/F_L < 0.001$). For this condition, wave propagation is forbidden in both directions, since nonlinearity acts as an open connection that reflects back the initial wave to the primary domain. On the other hand, for large-enough amplitudes ($F_0 > 9N$), the relative displacements of the masses in the nonlinear region are small ($Z_1 \simeq Z_2 \simeq Z_3$); hence the nonlinear springs act as rigid connections resulting in a reciprocal behavior accordingly. As illustrated in Fig. 2(c), when the initial wave propagates from left to

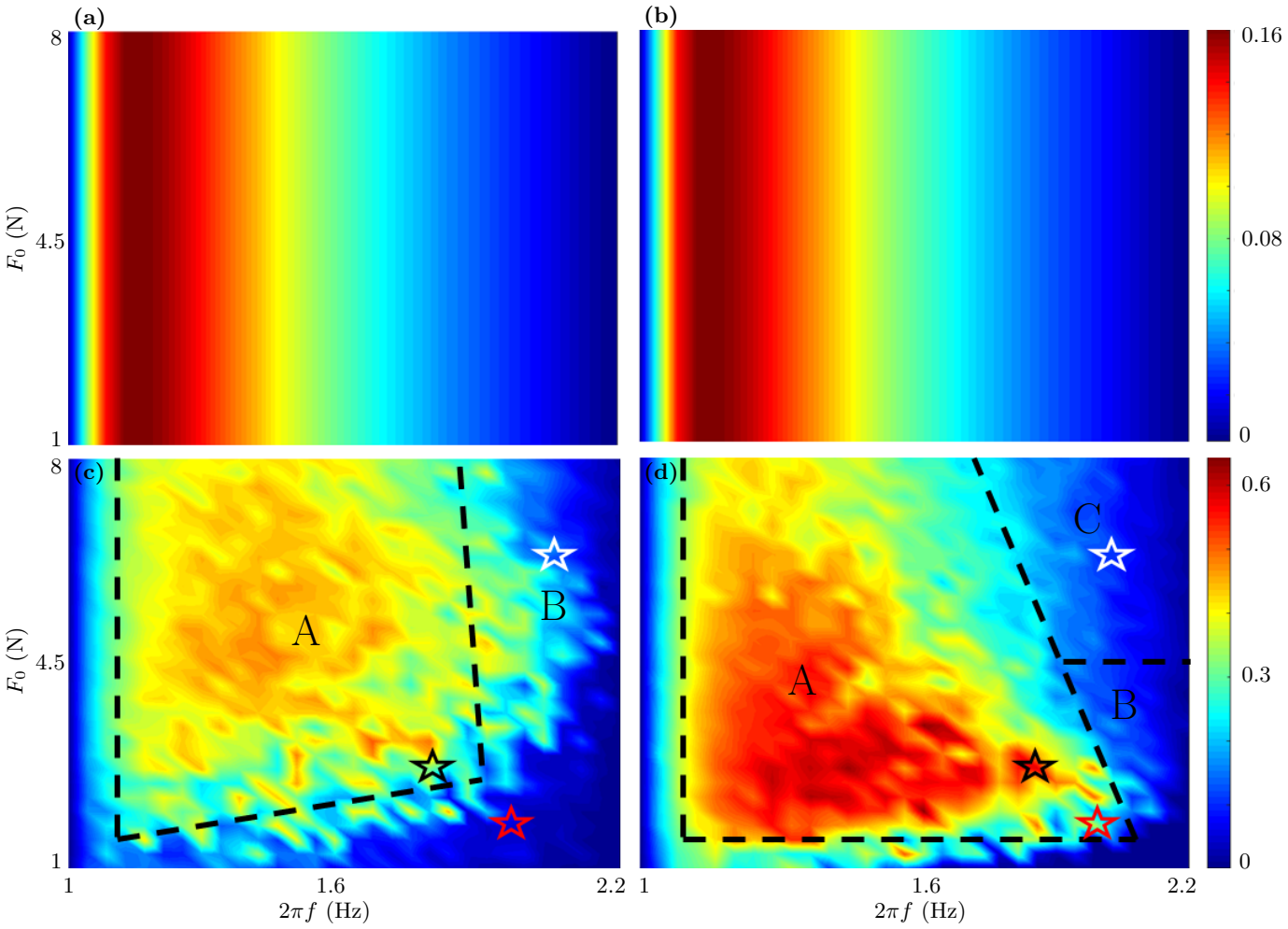

FIG. 2. **The normalized transmitted energy by sweeping input amplitude and frequency.** **(a)** Purely linear system when initial wave travels from left to right (LR), **(b)** Purely linear system when initial waves travel from right to left (RL), **(c)** Proposed system incorporating a nonlinear interface, when initial waves travel from left to right (LR), **(d)** Proposed system incorporating a nonlinear interface, when initial waves travel from right to left (RL). For the system with a nonlinear coupling, black dashed lines separate different non-reciprocity zones on the frequency-amplitude graphs. Note that, each of the stars in (c)-(d) represents a case with a different type of non-reciprocity.

right (LR), two domains of interest (A, B) are observed; while for the reverse direction, three domains (A, B, C) are observed (see Fig. 2(d)). In domain A, the amount of normalized transmitted wave is more than 5%, while domain B is defined where the value of η_i is less than 5%. In addition to these two domains, domain C is only defined for RL propagation, whereas the transmitted energy is less than 5%, but instead of the wave being reflected back, it is localized in the nonlinear gate (i.e., the nonlinear gate acts as an energy sink). These figures clearly indicate three different scenarios for non-reciprocity in the proposed system: i) waves propagate in both directions from the primary wave-guide to the secondary one, but with different amount of transmitted energies $(A-A)$, ii) waves propagate in one direction but the propagation is forbidden for the other direction $(B-A)$, and iii) waves are fully reflected without transmission for LR (i.e., 100% reflection), but wave is localized in the nonlinear gate for RL $(B-C)$. Each of these scenarios will be extensively analyzed in the following sections.

1. *A-A non-reciprocity*

Figure 3 plots the normalized transmitted energy over time for $F_0 = 2$, and $\omega = 2\pi f = 1.9$ (marked with black stars in Fig. 2) for both propagation directions. These plots demonstrate that when the primary wave propagates from left (right) to right (left), a portion of the left (right) domain energy transmits to the right (left) wave-guide, and the rest is reflected back to the primary domain. As shown, for both directions, the primary wave starts transmitting to the secondary domain until it reaches the steady level of energy at τ^*. Since the last cycle of the wave is reached to the coupling domain at τ^*, no wave will be sent to the nonlinear connection; therefore wave transmission is completed. For

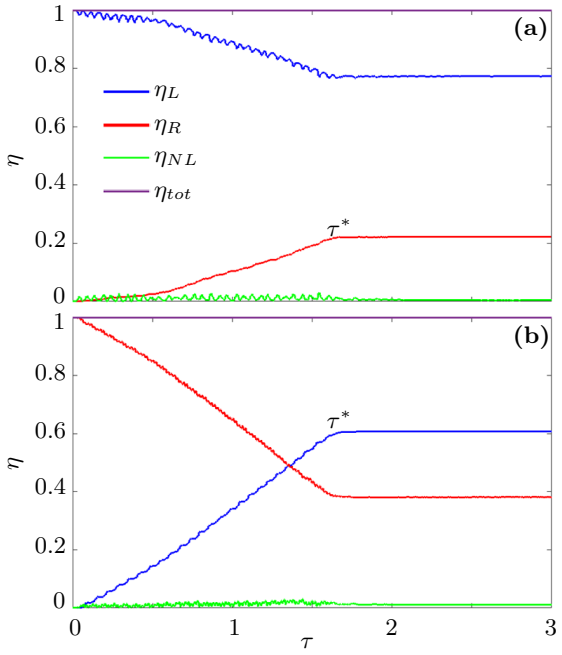

FIG. 3. **A-A energy transmission. (a)** Normalized transmitted energy for $F_0 = 2$ and $\omega = 2\pi f = 1.9$, when the initial wave propagates from left to right, **(b)** Normalized transferred energy for $F_0 = 2$ and $\omega = 2\pi f = 1.9$, when the initial wave propagates from right to left. For both graphs, blue represents the normalized energy of the left domain, red the right domain, green the nonlinear interface, and purple the total energy, respectively. Note that, this case is marked by black stars in Fig. 2(c),(d).

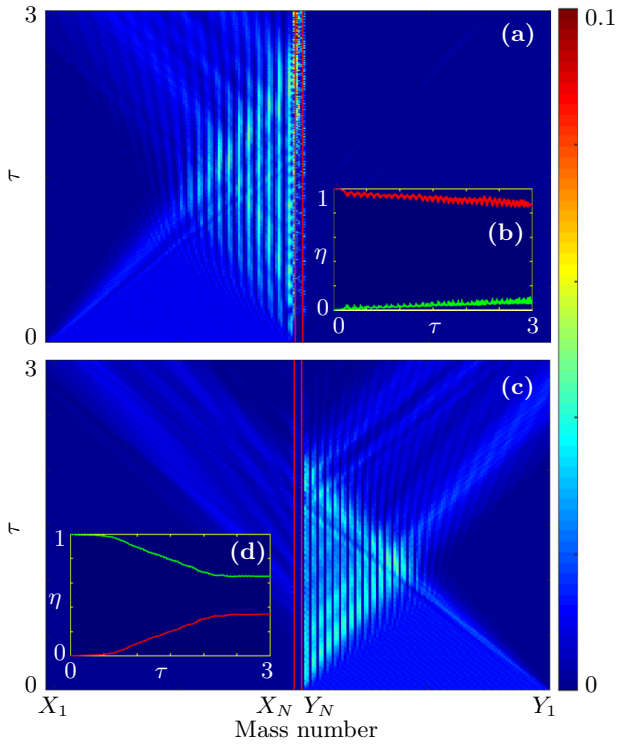

FIG. 4. **B-A spatio-temporal energy graphs. (a)** Energy distribution of each unit cell as a function of time and location, and **(b)** Normalized transferred energy for $F_0 = 1.6$ and $\omega = 2\pi f = 2.05$, when the initial wave propagates from left to right. **(c)** Energy distribution of each unit cell as a function of time and location, and **(d)** Normalized transferred energy for $F_0 = 1.6$ and $\omega = 2\pi f = 2.05$, when the initial wave propagates from right to left. For Figs. (b)-(d), green represents the normalized energy of the left domain, and red the normalized energy of the right domain, respectively. Note that, red vertical lines in Figs. (a)-(b) indicate the boundaries of the nonlinear interface.

both of these graphs, the total energy in the system is constant (i.e., $\eta_{tot} = 1$), which confirms no energy dissipation in the system. As observed in these graphs, when the structure is being excited on the left end, approximately $\eta_R = 22\%$ of the wave energy is transmitted to the secondary domain, while this value is $\eta_L = 61\%$ when the initial wave is generated on the right end of the structure. This difference between the transmitted energies documents a clear and strong non-reciprocity for opposite wave propagation directions, in which the energy transferred to the secondary subdomain for RL is 3 times of the same value for LR. Figure 2 in Supplementary Note 2 provides the fast Fourier transform (FFT) of signals at both input and output. As clearly shown, non-reciprocity is achieved with minimal frequency distortion of the sending signals. Furthermore, the spatio-temporal graphs are provided in Supplementary Note 3, where the propagation of the wave in the structure is depicted for both forward and backward directions.

2. B-A non-reciprocity

Figure 4 displays the energy transformation from the primary wave-guide to the secondary wave-guide for $F_0 = 1.6$ and $\omega = 2\pi f = 2.05$ (marked with red stars in Fig. 2(c)-(d)). As shown, waves propagate from the input on the right end to the output on the left end; while propagating in the reverse direction is forbidden. Figure 4(a)-(c) plot the energy of each mass in the structure depicted in Fig. 1. The energy for each mass, is the summation of the kinetic energy of the mass, and half of the potential energy of connected springs. As clearly documented in Fig. 4(a)-(b), for RL propagation, approximately 40% of the initial energy is transmitted to the left domain. Same as case $A - A$, this energy transformation from right to left happens without changing the frequency content of the original signal (see Fig. 4 in Supplementary Note 3). On the other hand, when the structure in Fig. 1 is excited from its left-end site, a very small portion of the energy is leaked to the left linear waveguide, and most of the propagating wave reflects back to the left side. Note that, the amount of transferred energy for this case is less than 5% without a dominant frequency in the FFT graph; therefore this energy leakage is negligible (see Supplementary Note 2 for more details).

3. B-C non-reciprocity

In this section, the most intriguing non-reciprocal behavior of the device is studied and analyzed. For this type of non-reciprocity, wave transmission is forbidden in both directions, but the wave can be localized at the location of the nonlinear springs only for RL propagation. Figures 5(a)-(b) plot the spatial temporal energy distribution of the structure for both propagation directions at $F_0 = 6$, $\omega = 2.1$ (marked with red stars in Fig. 2). Furthermore, the temporal variation of normalized energies in each domains are displayed in Figures 5(c)-(d). As depicted, for both propagation directions, less than 5% of the primary wave energy is transmitted to the secondary domain. Close inspection of these figures reveals that when the initial wave propagates from right to left, energy is trapped in the nonlinear gate (bounded by two red vertical lines in Fig. 5(b)). Figure 5(d) shows that approximately 20% of the initial energy is localized in the nonlinear domain. It should be noted that energy localization never happens for LR propagation for any choices of F_0, and f. This phenomenon (i.e., energy localization) can be employed in acoustic devices to design nonlinear energy sinks for vibration suppression, or energy harvesting purposes.

The next step to study this phenomenon is to analyze the incoming and outgoing forces on the nonlinear region. As such, for LR propagation, the force between X_{N-1} and X_N is defined as the input force (f_{LR}^{in}), and the one between Y_N, and Y_{N-1} is defined as the output force (f_{LR}^{out}), respectively. Similarly, for RL propagation, the force between Y_{N-1} and Y_N is defined as the input force (f_{RL}^{in}), and the one between X_N, and X_{N-1} is defined as the output force (f_{RL}^{out}) (see Supplementary Note 2 for more details). Figure 5(e-h) depicts the wavelet response of all of these forces for both propagation directions. As indicated, for LR propagation energy enters the nonlinear region at the frequency, equal to the excitation frequency ($\omega = 2\pi f = 2$), and later leaves the nonlinear region with minimal distortion. Since this frequency lies in the band-pass of the right wave-guide (marked with red dashed lines), waves propagate into this domain without being trapped at the nonlinear region. Conversely, for RL propagation, f_{in}^{RL} has a frequency component outside the band-pass of both wave-guides, which rises over time. Accordingly, this part of the signal can not propagate into any of the wave-guides, and will be trapped in the nonlinear region. One possible reason for such behavior is the impedance mismatch between Z_3 and Y_N, when the wave travels from right to left, while this is not happening for the other direction of propagation. A detailed investigation of the energy localization is provided in Supplementary Note 2, by studying wavelet-bounded empirical mode decomposition (WBEMD), and nonlinear normal modes (NNMs) of the nonlinear interface.

B. Experimental results

In this section, a set of experiments is performed to confirm the performance of the proposed non-reciprocal structure. The experimental structure depicted in Fig. 6 is formed by connecting 9 aluminum masses, where the masses at either ends are excited by 10 cycles of harmonic velocity (see Supplementary Note 5 for full details on the experimental setup, parameters, and system identifications). Figure 7(a-b) exhibit snapshots of the experimentally measured velocity in response to excitation $V_0 = 2sin(30 \times 2\pi t)\ mm/s$. The provided subfigures clearly confirm non-reciprocity, where the response of the output for RL is 8 times larger than that for LR. Figure 7(c) provides the frequency response of both outputs for the same excitation condition. As observed, waves at the output for both directions propagate almost at the same frequency as the input; however the amplitude of the wave for RL is much higher than the opposite direction. As another example, the responses of the system for $V_0 = 1.5sin(40 \times 2\pi t)\ mm/s$ are depicted in Figure 7(d-f). For this example excitation, the frequency response of the output for LR does not contain a dominant peak, while for RL the FFT graph clearly demonstrate a dominant peak at $f = 40\ Hz$. These two examples clearly confirm the potential of the proposed design to obtain non-reciprocal responses for different propagation directions.

In summary, this work proposed and studied a passive broad-band acoustic non-reciprocal structure. The introduced system was composed of two identical linear wave-guides coupled with a nonlinear interface. This nonlinear domain contained unequal masses, and nonlinear springs. First, the transmitted energy for broad ranges of input amplitude and frequency was plotted, and compared with a purely linear system, documenting a clear non-reciprocity for opposite propagation directions. Later, three different types of non-reciprocity in the proposed system were studied and analyzed. Furthermore, energy localization for backward propagation was theoretically investigated by studying the intrinsic mode functions, and nonlinear normal modes of the finite system. Finally, a set of experiments was carried-out to verify the performance of the system in breaking the acoustic reciprocity.

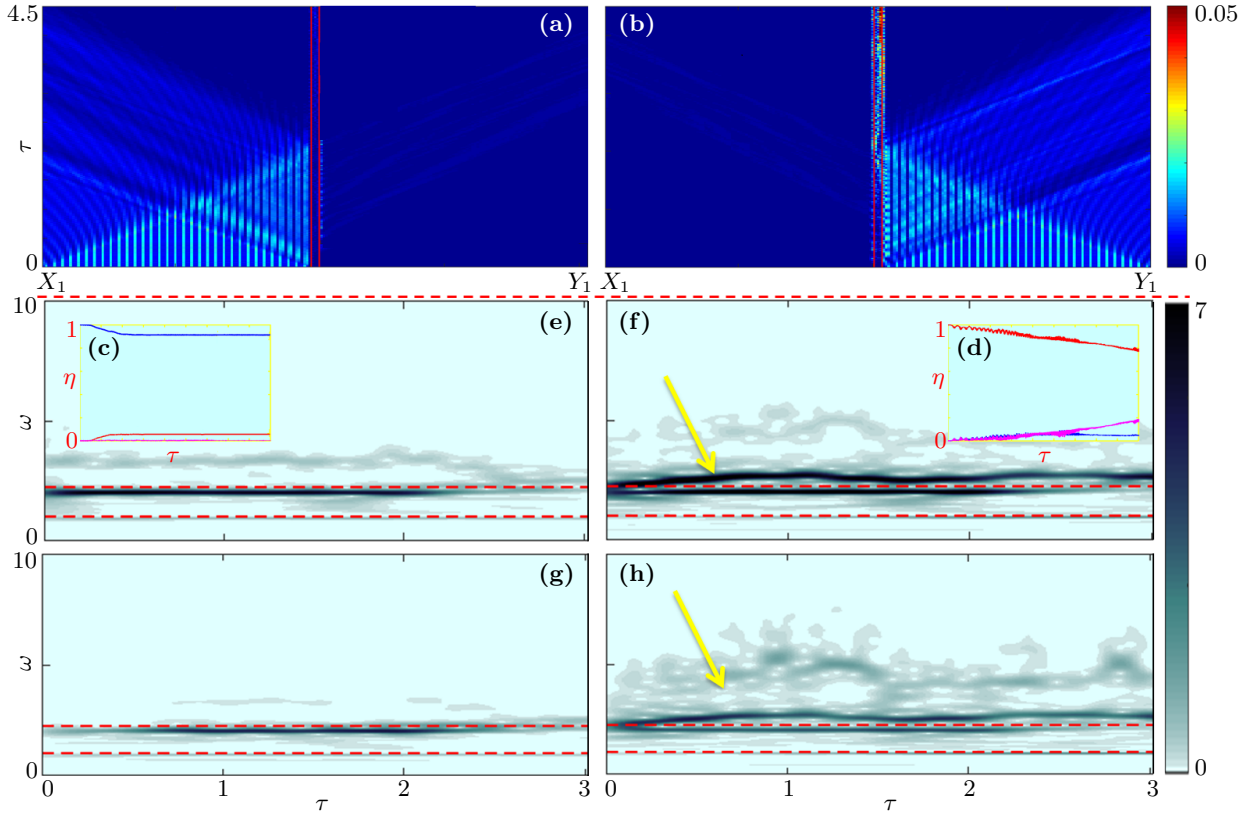

FIG. 5. **B-C energy localization. (a)-(b)** Spatio-temporal energy distribution of each unit cell, **(c)-(d)** Normalized energy of each domain as a function of time, **(e)-(f)** Wavelet response of the input force entering the nonlinear gate, and **(g)-(h)** Wavelet response of the output force leaving the nonlinear domain, at $F_0 = 6$, and $\omega = 2\pi f = 2.1$. Note that, the graphs on the left (right) side represent the condition, in which the initial waves propagate from left (right) to right (left). In addition, in Figs. (c)-(d), blue represents the normalized energy of the left domain, red the normalized energy of the right domain, and purple the normalized energy of the nonlinear domain, respectively. Also, red horizontal dashed lines in Figs. (e-h) indicate the pass-band boundaries of the linear wave-guides, and yellow arrows indicate the created mode outside of the pass-band, respectively.

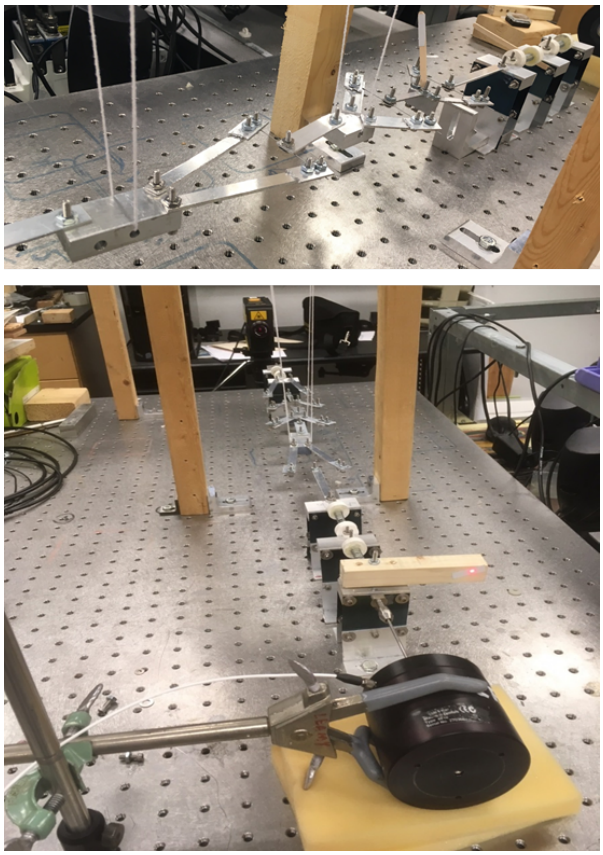

FIG. 6. **Experimental setup.** Schematic of the experimental setup.

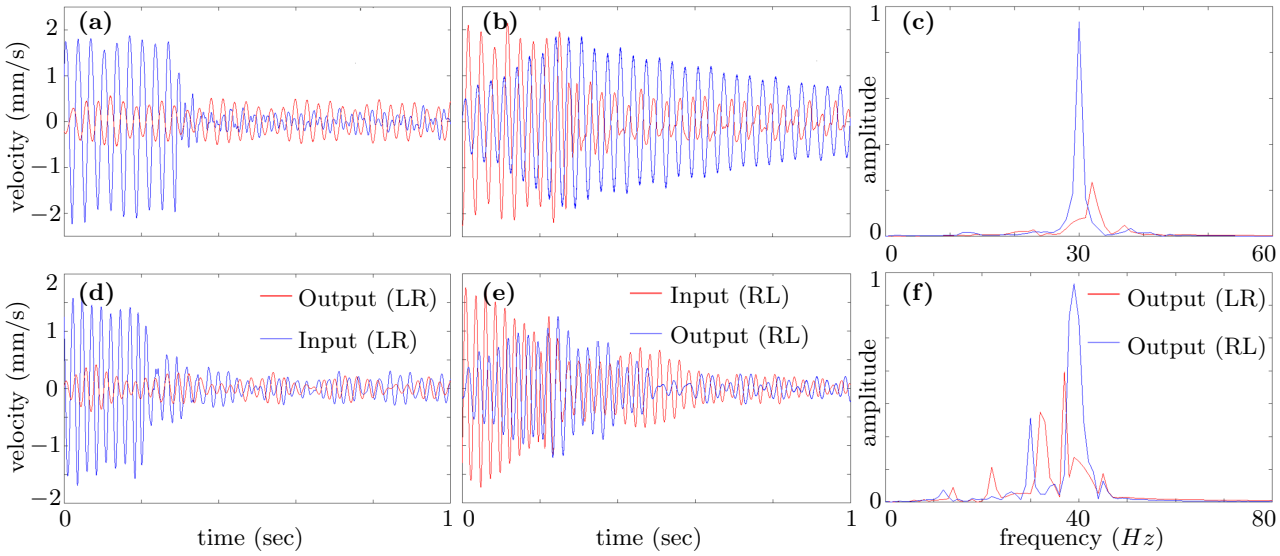

FIG. 7. **Experimental results.** **(a)** Experimentally measured wave response of the signals at input and output, when the source is on the left end, **(b)** Experimentally measured wave response of the input and output, when the source is on the right end, **(c)** Frequency response of the outputs for both propagation directions when $V_0 = 2sin(30 \times 2\pi t)\ mm/s$. **(d)** Experimentally measured wave response of the input and output, when the source is on the left end, **(e)** Experimentally measured wave response of the signals at input and output, when the source is on the right end, and **(f)** Frequency response of the outputs for both propagation directions when $V_0 = 2sin(30 \times 2\pi t)\ mm/s$. For all of these plots, blue lines represent the response of the first mass on the left side (X_1), and red lines represent the response of the first mass on the right side (Y_1). Note that, for the frequency graphs, the amplitude of the signal is normalized with respect to the higher peak.

[1] H. B. G. Casimir, On onsager's principle of microscopic reversibility, Reviews of Modern Physics **17**, 343 (1945).

[2] L. Onsager, Reciprocal relations in irreversible processes. i., Physical review **37**, 405 (1931).

[3] H. v. Helmholtz, Theorie der luftschwingungen in rohren mit offenen enden, Journal fur die reine und angewandte Mathematik **57**, 1 (1860).

[4] J. Strutt, Some general theorems relating to vibrations, Proceedings of the London Mathematical Society **1**, 357 (1871).

[5] S. A. Cummer, J. Christensen, and A. Alù, Controlling sound with acoustic metamaterials, Nature Reviews Materials **1**, 16001 (2016).

[6] D. Monroe, Focus: One-way mirror for sound waves, Physics **24**, 8 (2009).

[7] A. Darabi and M. J. Leamy, Clearance-type nonlinear energy sinks for enhancing performance in electroacoustic wave energy harvesting, Nonlinear Dynamics **87**, 2127 (2017).

[8] V. Nesterenko, C. Daraio, E. Herbold, and S. Jin, Anomalous wave reflection at the interface of two strongly nonlinear granular media, Physical review letters **95**, 158702 (2005).

[9] B. Li, L. Wang, and G. Casati, Thermal diode: Rectification of heat flux, Physical review letters **93**, 184301 (2004).

[10] M. Terraneo, M. Peyrard, and G. Casati, Controlling the energy flow in nonlinear lattices: a model for a thermal rectifier, Physical Review Letters **88**, 094302 (2002).

[11] B. Li, J. Lan, and L. Wang, Interface thermal resistance between dissimilar anharmonic lattices, Physical review letters **95**, 104302 (2005).

[12] R. Fleury, D. L. Sounas, C. F. Sieck, M. R. Haberman, and A. Alù, Sound isolation and giant linear nonreciprocity in a compact acoustic circulator, Science **343**, 516 (2014).

[13] X. Zhang and Z. Liu, Extremal transmission and beating effect of acoustic waves in two-dimensional sonic crystals, Physical review letters **101**, 264303 (2008).

[14] S. H. Mousavi, A. B. Khanikaev, and Z. Wang, Topologically protected elastic waves in phononic metamaterials, Nature communications **6**, 8682 (2015).

[15] K. Tsakmakidis, L. Shen, S. Schulz, X. Zheng, J. Upham, X. Deng, H. Altug, A. Vakakis, and R. Boyd, Breaking lorentz reciprocity to overcome the time-bandwidth limit in physics and engineering, Science **356**, 1260 (2017).

[16] R. Fleury, D. Sounas, and A. Alù, An invisible acoustic sensor based on parity-time symmetry, Nature communications **6**, 5905 (2015).

[17] D. L. Sounas, C. Caloz, and A. Alu, Giant non-reciprocity at the subwavelength scale using angular momentum-biased metamaterials, Nature communications **4**, 2407 (2013).

[18] A. Kamal, J. Clarke, and M. Devoret, Noiseless non-reciprocity in a parametric active device, Nature Physics **7**, 311 (2011).

[19] N. A. Estep, D. L. Sounas, J. Soric, and A. Alù, Magnetic-free non-reciprocity and isolation based on parametrically modulated coupled-resonator loops, Nature Physics **10**, 923 (2014).

[20] B. Liang, X. Guo, J. Tu, D. Zhang, and J. Cheng, An acoustic rectifier, Nature materials **9**, 989 (2010).

[21] C. Coulais, D. Sounas, and A. Alù, Static non-reciprocity in mechanical metamaterials, Nature **542**, 461 (2017).

[22] X.-F. Li, X. Ni, L. Feng, M.-H. Lu, C. He, and Y.-F. Chen, Tunable unidirectional sound propagation through a sonic-crystal-based acoustic diode, Physical review letters **106**, 084301 (2011).

[23] Z. Wu, Y. Zheng, and K. Wang, Metastable modular metastructures for on-demand reconfiguration of band structures and nonreciprocal wave propagation, Physical Review E **97**, 022209 (2018).

[24] Z. Wu and K.-W. Wang, On the wave propagation analysis and supratransmission prediction of a metastable modular metastructure for non-reciprocal energy transmission, arXiv preprint arXiv:1709.03229 (2017).

[25] N. Boechler, G. Theocharis, and C. Daraio, Bifurcation-based acoustic switching and rectification, Nature materials **10**, 665 (2011).

[26] H. Nassar, X. Xu, A. Norris, and G. Huang, Modulated phononic crystals: Non-reciprocal wave propagation and willis materials, Journal of the Mechanics and Physics of Solids **101**, 10 (2017).

[27] G. Trainiti and M. Ruzzene, Non-reciprocal elastic wave propagation in spatiotemporal periodic structures, New Journal of Physics **18**, 083047 (2016).

[28] Y. Zheng, Z. Wu, X. Zhang, and K. Wang, A piezo-metastructure with bistable circuit shunts for adaptive nonreciprocal wave transmission, arXiv preprint arXiv:1812.00517 (2018).

[29] B.-I. Popa and S. A. Cummer, Non-reciprocal and highly nonlinear active acoustic metamaterials, Nature communications **5**, 3398 (2014).

[30] N. Li and J. Ren, Non-reciprocal geometric wave diode by engineering asymmetric shapes of nonlinear materials, Scientific reports **4**, 6228 (2014).

[31] B. Liang, B. Yuan, and J.-c. Cheng, Acoustic diode: Rectification of acoustic energy flux in one-dimensional systems, Physical review letters **103**, 104301 (2009).

[32] I. Grinberg, A. F. Vakakis, and O. V. Gendelman, Acoustic diode: Wave non-reciprocity in nonlinearly coupled waveguides, Wave Motion **83**, 49 (2018).

[33] K. J. Moore, J. Bunyan, S. Tawfick, O. V. Gendelman, S. Li, M. Leamy, and A. F. Vakakis, Nonreciprocity in the dynamics of coupled oscillators with nonlinearity, asymmetry, and scale hierarchy, Physical Review E **97**, 012219 (2018).

[34] J. Bunyan, K. J. Moore, A. Mojahed, M. D. Fronk, M. Leamy, S. Tawfick, and A. F. Vakakis, Acoustic nonreciprocity in a lattice incorporating nonlinearity, asymmetry, and internal scale hierarchy: Experimental study, Physical Review E **97**, 052211 (2018).

[35] M. D. Fronk, S. Tawfick, C. Daraio, A. F. Vakakis, and M. J. Leamy, Non-reciprocity in structures with nonlinear internal hierarchy and asymmetry, in *ASME 2017 International Design Engineering Technical Conferences and Computers and Information in Engineering Conference* (American Society of Mechanical Engineers 2017), pp. V008T12A023–V008T12A023.

[36] A. Mojahed, K. Moore, L. A. Bergman, and A. F. Vakakis, Strong geometric softening-hardening nonlinearities in an oscillator composed of linear stiffness and

damping elements, International Journal of Non-Linear Mechanics (2018).

[37] A. F. Vakakis, O. V. Gendelman, L. A. Bergman, D. M. McFarland, G. Kerschen, and Y. S. Lee, *Nonlinear targeted energy transfer in mechanical and structural systems*, volume 156 (Springer Science & Business Media 2008).

[38] Y. S. Lee, G. Kerschen, A. F. Vakakis, P. Panagopoulos, L. Bergman, and D. M. McFarland, Complicated dynamics of a linear oscillator with a light, essentially nonlinear attachment, Physica D: Nonlinear Phenomena **204**, 41 (2005).

[39] T. Revannasiddaiah and R. Kumar, Modal interactions and targeted energy transfers in laminar vortex-induced vibrations of a rigid cylinder with strongly nonlinear internal attachments, Ph.D. thesis, University of Illinois at Urbana-Champaign (2014).

[40] O. V. Gendelman, A. F. Vakakis, L. A. Bergman, and D. M. McFarland, Asymptotic analysis of passive nonlinear suppression of aeroelastic instabilities of a rigid wing in subsonic flow, SIAM Journal on Applied Mathematics **70**, 1655 (2010).

[41] C.-H. Lamarque and A. T. Savadkoohi, Dynamical behavior of a bouc–wen type oscillator coupled to a nonlinear energy sink, Meccanica **49**, 1917 (2014).

[42] A. F. Vakakis, M. A. AL-Shudeifat, and M. A. Hasan, Interactions of propagating waves in a one-dimensional chain of linear oscillators with a strongly nonlinear local attachment, Meccanica **49**, 2375 (2014).

[43] J. Shao and B. Cochelin, Theoretical and numerical study of targeted energy transfer inside an acoustic cavity by a non-linear membrane absorber, International Journal of Non-Linear Mechanics **64**, 85 (2014).